

A Strategy for Preparing Quantum Squeezed States Using Reinforcement Learning

X. L. Zhao*, Y. M. Zhao, M. Li, T. T. Li, Q. Liu, S. Guo,¹ and X. X. Yi²

¹*School of Science, Qingdao University of Technology, Qingdao 0532, China*

²*Center for Quantum Sciences and School of Physics,
Northeast Normal University, Changchun 130024, China*

(Dated: June 11, 2024)

We propose a scheme leveraging reinforcement learning to engineer control fields for generating non-classical states. It is exemplified by the application to prepare spin-squeezed states for an open collective spin model where a linear control field is designed to govern the dynamics. The reinforcement learning agent determines the temporal sequence of control pulses, commencing from a coherent spin state in an environment characterized by dissipation and dephasing. Compared to the constant control scenario, this approach provides various control sequences maintaining collective spin squeezing and entanglement. It is observed that denser application of the control pulses enhances the performance of the outcomes. However, there is a minor enhancement in the performance by adding control actions. The proposed strategy demonstrates increased effectiveness for larger systems. Thermal excitations of the reservoir are detrimental to the control outcomes. Feasible experiments are suggested to implement this control proposal based on the comparison with the others. The extensions to continuous control problems and another quantum system are discussed. The replaceability of the reinforcement learning module is also emphasized. This research paves the way for its application in manipulating other quantum systems.

I. INTRODUCTION

Precise measurement for physical quantities propels the progress of physics. The utilization of non-classical quantum states facilitates the pathway towards achieving precise measurements. Spin-squeezed states are such non-classical candidates characterized by reduced uncertainty in a collective spin component. Entanglement typically arises concomitantly with spin squeezing, as a result of the nonlinear interactions within an ensemble [1, 2]. Reducing the variance of an observable enhances measurement sensitivity, surpassing the standard quantum limit in the domain of quantum-enhanced metrology. Such squeezed states can be used to enhance the performance of homodyne interferometers [3, 4], magnetometers [5], and atomic clocks [6]. The evidence delineating the association between the sensitivity of phase estimation and entanglement was demonstrated by a collective spin model [7].

Many schemes have been proposed to prepare spin-squeezed states [1, 2, 8]. For example, quantum non-demolition measurement can be used to generate spin-squeezed states [9]. Theoretically, a coherent control method has been proposed to produce spin-squeezed states [10]. Some proposals are based on the nonlinear interaction among the individual elements in Bose-Einstein condensates [11–14]. Proposals which can prepare long-lasting and extreme spin-squeezed states are pursued all the way.

Machine-learning techniques are emerging as effective tools in physics [15–17], and among them, reinforcement learning (RL) offers the potential to optimize the control field for high-dimensional, multistage processes in complex scenarios. Deep reinforcement learning (DRL) can provide a control strategy to engineer the dynamics as long as the evolution follows certain differential

equations. In physics, many optimal problems can be treated as control problems of finding means to steer a system to achieve a certain target. The search for optimal control fields can be formulated as RL tasks [17–19]. A semiquantum reinforcement learning approach is employed to adapt a qubit to an unknown state by successive single-shot measurements and feedback [20]. A four-step strategy combining constant-value and time-varying controls results in an enhanced longtime stable spin squeezing for a collective spin system coupled to a bosonic field [21]. A measurement-based adaptation protocol is introduced to optimize a quantum state for maximum overlap with an unknown reference state using quantum reinforcement learning [22]. This study provides a foundational framework for the development of quantum reinforcement learning protocols leveraging quantum data.

We mainly propose an RL-based control scheme to design the control field to prepare non-classical spin states. The agent is trained to produce a sequence of square pulses that steer the system to squeezed states under the domain of a Lindblad master equation. This control method can be regarded as a kind of combination of bang-bang control [23, 24] and reinforcement learning. The performance of the proposed control scheme is evaluated across a range of control parameters, system size, and thermal excitations.

This paper is organized as follows: In Sec.II, we delineate the reinforcement-learning-based framework to prepare nonclassical states. In Sec.III, the RL module employed within the control scheme is shown. In Sec.IV, we explicate the quantum model for the generation of spin-squeezed states. In Sec.V, we present the procedure to prepare squeezed states of the open collective spin system via reinforcement learning. In Sec.VI, we check the performance of this method including the influence of the

frequency of applying the control pulses, the granularity of control actions, the scalability across various sizes, the impact of thermal excitation, and the comparison with other current protocols. In Sec.VII, we discuss the feasibility of this control scheme in terms of BEC experiments, the application to continuous control situations and the extension to another quantum system. The replaceability of the RL agent is also discussed. Finally, we conclude in Sec.VIII.

II. CONTROL SCHEME

Taking a cue from Lyapunov control strategies [25–29], we propose a scheme harnessing an RL agent to design the control fields to prepare nonclassical states. In the presence of control fields, the general total Hamiltonian for the quantum system reads: $\hat{H} = \hat{H}_0 + \sum_{m=1}^M f_m(t)\hat{H}_m$, where \hat{H}_0 is the free Hamiltonian and M denotes the amount of the external control Hamiltonians \hat{H}_m . $f_m(t)$ is the control field designed by the RL agent. It should be confirmed that $[\hat{H}_0, \hat{H}_m] \neq 0$, otherwise, the influence of the control Hamiltonians can be subsumed into the free Hamiltonian.

This is an open-loop strategy in application, wherein the control fields are determined through the emulation of a closed-loop process, as shown in Fig. 1. Under the control designed by the machine learning agent, the system would be steered to a set of states meeting the control target. Notably, the RL agent can be supplanted by other optimization modules tailored to the target. The proposed control scheme can be applied to other dynamical systems governed by certain differential equations. To illustrate the efficacy of the scheme, we have applied it to engineer a collective spin system.

III. MACHINE LEARNING TOOLS: REINFORCEMENT LEARNING

Initiating with no prior knowledge about the system under control, RL adopts the trial-and-error paradigm to iteratively learn the mapping between the action and the state with maximal accumulated reward over time instances. Rewards are obtained using an evaluation rule that aligns with the control objectives. An appropriate rewards-evaluation rule that favors particular state-action mappings can enhance the control performance. Decision-making executed by the agent entails selecting actions $a_t = \pi(s_t)$ that affect the system changing from a state (not specifically referring to quantum states, but a general state characterized by various quantities of a controlled system) s_t to s_{t+1} , with π denoting the policy being learned [15–17].

Q-learning works through a Q function which represents the expected total future reward of a policy π . The optimal policy π^* with maximized Q function satisfies

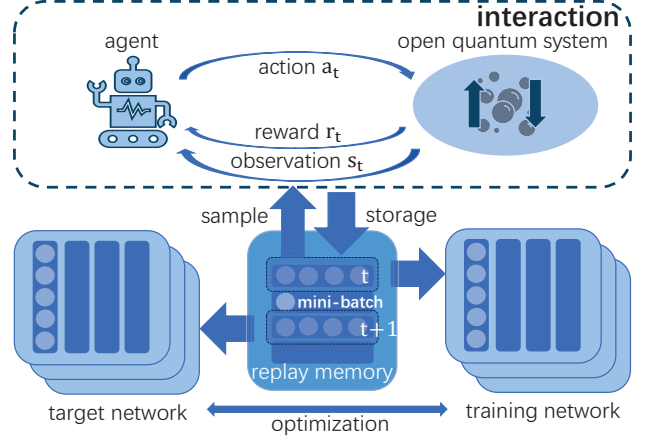


Figure 1. The schematic of the training procedure: 1. The agent provides actions a_t to steer the open quantum system (the ‘environment’ in RL), and receives observations s_t and rewards r_t . 2. These experiences are stored in the replay memory as a state-action-reward combination of the mapping. 3. The agent is trained to minimize the difference between the predicted Q values and the target Q values. 4. The target Q values are computed by considering the immediate reward and the estimated maximum future rewards. 5. The process including interaction, experience replay, and network updates is repeated to iteratively improve the Q-function approximation.

Bellman equation [30, 31] which encapsulates the principle of optimality for decision-making over time. Deep Q-learning uses a deep neural network to approximate this function [32–34], and the network is called a deep Q network (DQN).

In DQN, the Q function is defined as

$$Q^\pi(s_t, a_t) = r(s_t) + E_{\{(s_{t+k}, a_{t+k}) | \pi\}_{k=1}^{\infty}} \left[\sum_{k=1}^{\infty} \gamma_q^k r(s_{t+k}) \right] \quad (1)$$

where $r(s_t)$ is the reward at episode t when the state is s_t , γ_q^k ($0 < \gamma_q^k < 1$, usually close to 1) is a discount factor, and the expectation $E_{\{\dots\}}[\dots]$ is taken over trajectories of the actions and the states of the controlled system [30, 31]. The Q function is implemented during training based on the structure of the agent. When the Bellman equation

$$Q^{\pi^*}(s_t, a_t) = r(s_t) + \gamma_q E_{s_{t+1}} \left[\max_{a_{t+1}} Q^{\pi^*}(s_{t+1}, a_{t+1}) \right] \quad (2)$$

for $\gamma_q^k = \gamma_q \approx 1$, is satisfied by training, the optimal policy π^* (state-action mapping) is determined. Deep Q-learning employ a neural network, denoted by $W_\theta(s, a)$, to approximate Q^{π^*} [32, 33], where θ represents the network parameters that need to be adjusted by training. After training, $W_\theta(s, a)$ approximates Q^{π^*} by adjusting the parameters θ so that Eq. (2) is satisfied. Then the optimal policy π^* be found.

DQN leverages extensive datasets that encapsulate the anticipated cumulative rewards consequent to spe-

cific actions within distinct states, facilitating the neural network-based approximation of the conventional action-value function [32–38]. It should be noted that depending on particular needs and constraints of tasks, alternative optimization algorithms could be employed in place of the DQN.

IV. COLLECTIVE SPIN MODEL

We consider an ensemble of N identical two-level atoms with pseudo spin components $\hat{J}_\alpha = \frac{1}{2} \sum_{k=1}^N \hat{\sigma}_\alpha^{(k)}$, ($\alpha = x, y, z$), where $\hat{\sigma}_\alpha^{(k)}$ is the Pauli operator for the k -th atom [39]. This is the symmetric scenario where the operations done on the ensemble have identical impact on all the atoms. $\hat{J}_x, \hat{J}_y, \hat{J}_z$ fulfill the SU(2) commute relationship: $[\hat{J}_\alpha, \hat{J}_\beta] = i\hbar\epsilon_{\alpha\beta\gamma}\hat{J}_\gamma$, where $\epsilon_{\alpha\beta\gamma}$ is the Lévi-Civita symbol. The total collective spin length is specified by $J = N/2$ and the dimension of the Hilbert space is $2J+1 = N+1$. The collective spin can be mapped to its two-mode bosonic partner by Schwinger transformation: $\hat{J}_z = \frac{1}{2}(\hat{a}^\dagger\hat{a} - \hat{b}^\dagger\hat{b})$, $\hat{J}_+ = \hat{a}^\dagger\hat{b}$ and $\hat{J}_- = (\hat{J}_+)^\dagger$, where \hat{a} and \hat{b} are the two annihilation operators of two boson modes. Namely, $\hat{J}_x = (\hat{J}_+ + \hat{J}_-)/2$, and $\hat{J}_y = (\hat{J}_+ - \hat{J}_-)/2i$ [40]. In this view, by mapping one mode to spin up and the other one to spin down, \hat{J}_z reflects the population difference between the two modes in Ramsey interferometer [2, 3, 8].

To examine the efficacy of the strategy, we focus on a collective spin system described by the Hamiltonian

$$\hat{H}/\hbar = \kappa\hat{J}_z^2 + \Omega_x(t)\hat{J}_x, \quad (3)$$

here κ indicates the strength of the interaction between the atoms and the time scales as κt . κ would be taken as the unit ($\kappa = 1$ hereafter) and the natural units ($\hbar = 1$) is used. \hat{J}_z^2 refers to the one-axis twisting which induces spin squeezing [8]. This squeezing provides the resource for quantum-enhanced metrology [2, 8]. \hat{J}_x is the control Hamiltonian describing the magnetic field in the x -direction, or the counterpart, the linear beam splitter in interferometers.

In contrast to the application of a constant control [10], the present proposal employs an RL agent designing time-dependent control field $\Omega_x(t)$ to prepare nonclassical states. The temporally varying control field can represent the operational analogy of linear beam splitters in interferometric experiments [13, 14]. Since $[\hat{J}_z^2, \hat{J}_x] = i(\hat{J}_y\hat{J}_z + \hat{J}_z\hat{J}_y)$, such a linear control Hamiltonian can be used to steer the spin system.

Spin squeezing can be quantified by parameters constructed by the expected values of collective spin operators [1, 2]. Upon the reduction of the variances beneath the standard quantum limit threshold, the system is rendered applicable for precision metrology, along with amplifying the variance of the orthogonal spin components. We should confirm that the minimum squeezing param-

eter reads

$$\xi_\perp^2 = \frac{N \min(\Delta\hat{J}_{\vec{n}_\perp}^2)}{|\langle\hat{J}_s\rangle|^2} = \frac{N \left[\langle\hat{J}_{\vec{n}_1}^2 + \hat{J}_{\vec{n}_2}^2\rangle - \sqrt{\langle\hat{J}_{\vec{n}_1}^2 - \hat{J}_{\vec{n}_2}^2\rangle^2 + \langle[\hat{J}_{\vec{n}_1}, \hat{J}_{\vec{n}_2}]_+\rangle^2} \right]}{2|\langle\hat{J}_s\rangle|^2}, \quad (4)$$

where $\hat{J}_{\vec{n}_i} = (\hat{J}_x, \hat{J}_y, \hat{J}_z) \cdot \vec{n}_i$, ($i = 1, 2$) and $\vec{n}_1 = (-\sin\phi, \cos\phi, 0)$, $\vec{n}_2 = (\cos\theta\cos\phi, \cos\theta\sin\phi, -\sin\theta)$. The collective spin operator $\hat{J}_s = (\hat{J}_x, \hat{J}_y, \hat{J}_z) \cdot (\sin\theta\cos\phi, \sin\theta\sin\phi, \cos\theta)$, where $\theta = \arccos(\frac{\langle\hat{J}_z\rangle}{|J|})$, $\phi = \text{sign}(\langle\hat{J}_y\rangle) \arccos(\frac{\langle\hat{J}_x\rangle}{|J|\sin\theta})$, the norm $|J| = \sqrt{\langle\hat{J}_x\rangle^2 + \langle\hat{J}_y\rangle^2 + \langle\hat{J}_z\rangle^2}$ [1, 2, 41]. Here the direction $\vec{n}_\perp = \vec{n}_1\cos\varphi + \vec{n}_2\sin\varphi$ with

$$\varphi = \begin{cases} \frac{1}{2} \arccos\left(\frac{-A}{\sqrt{A^2+B^2}}\right) & \text{if } B \leq 0, \\ \pi - \frac{1}{2} \arccos\left(\frac{-A}{\sqrt{A^2+B^2}}\right) & \text{if } B > 0, \end{cases} \quad (5)$$

where $A \equiv \langle\hat{J}_{\vec{n}_1}^2 - \hat{J}_{\vec{n}_2}^2\rangle$, $B \equiv \langle[\hat{J}_{\vec{n}_1}, \hat{J}_{\vec{n}_2}]_+\rangle$.

In this control scheme, we employ the following definition

$$\xi_Z^2 = \frac{N\Delta\hat{J}_z^2}{|\langle\hat{J}_s\rangle|^2}, \quad (6)$$

as the squeezing parameter. Here $\Delta\hat{J}_z^2 = \langle\hat{J}_z^2\rangle - \langle\hat{J}_z\rangle^2$, indicates the spin squeezing in the z -direction. For the RL, we use the reverse of ξ_Z^2 to set the reward-punishment rule during the control process. The reward function we use is $R = 10\langle\Delta R_t \leq 0\rangle - \langle\Delta R_t < 0\rangle$, where

$$\langle\bullet\rangle = \begin{cases} -1 & \text{if } \bullet \leq 0, \\ 1 & \text{if } \bullet > 0, \end{cases} \quad (7)$$

$\Delta R_t = \frac{1}{\xi_z^2(t+1)} - \frac{1}{\xi_z^2(t)}$. Here $\frac{1}{\xi_z^2(t)}$ is the inverse of the squeezing parameter at the sample time t during training. This reward function means that the agent gets 10 points if the action makes the squeezing parameter decrease, whereas deduct 1 point if the squeezing parameter rises. Subsequently, in accordance with the fundamental principles of RL, the agent will steer the direction with minimum squeezing parameter approaching the z direction, namely, $\varphi = \pi/2$ in Eq. (5). Compared to using the reverse of ξ_R^2 with variable θ and ϕ , the choice of ξ_Z^2 possesses a more direct physical interpretation since \hat{J}_z signifies the population imbalance between the two modes within the Ramsey interferometer mentioned above [2, 3, 8].

Correlation exists between entanglement and spin squeezing [42], wherein multipartite entanglement constitutes a quantum resource for enhanced precision in

metrology [7, 43]. Moreover, quantum Fisher information (QFI) quantifies the link between entanglement and phase uncertainty within the domain of metrology [44, 45]. Adhering to the quantum Cramer-Rao bound, quantum states with larger QFI are pursued for the precision of quantum metrology [46, 47]. We would check the QFI about the spin state $\hat{\rho}$ concerning $\hat{\rho}(\delta) = e^{i\delta\hat{G}}\hat{\rho}e^{-i\delta\hat{G}}$, where δ is the quantity which needs to be estimated with respect to the phase-shift operator \hat{G} [48, 49]. The QFI reads

$$F(\rho, \hat{G}) = 4 \sum_n p_n (\Delta \hat{G})_n^2 - \sum_{m \neq n} \frac{8p_m p_n}{p_m + p_n} |\langle \psi_m | \hat{G} | \psi_n \rangle|^2, \quad (8)$$

where $\rho |\psi_n\rangle = p_n |\psi_n\rangle$, $(\Delta \hat{G})_n^2 \equiv \langle \psi_n | \hat{G}^2 | \psi_n \rangle - |\langle \psi_n | \hat{G} | \psi_n \rangle|^2$. The second term denotes a correction. Here, QFI provides a quantitative threshold for the precision attainable in estimating δ by measuring \hat{G} on ρ . If the average QFI over three basic directions reaches the order of 1, there is macroscopic multi-particle entanglement [50]. A comprehensive solution for QFI calculation has already been integrated into the package QuanEstimation [51].

V. PREPARE SPIN-SQUEEZED STATE BY REINFORCEMENT LEARNING

There are mainly two steps to prepare the spin-squeezed states: firstly, a spin coherent state should be prepared, and secondly, a spin-squeezed state is prepared by using a control field designed by a machine learning agent.

A. Initial coherent spin state

N two-level atoms all pointing along the same direction can be described by SU(2) coherent spin state (CSS). Such a state reads

$$|\theta, \phi\rangle = (\cos \frac{\theta}{2})^{2j} \sum_{m=-j}^j (C_{j+m}^{2j})^{1/2} [e^{-i\phi} \tan \frac{\theta}{2}]^{j+m} |j, m\rangle, \quad (9)$$

where C_{j+m}^{2j} are the binomial coefficients. This overcomplete state is most similar to the classical one with θ and ϕ being the azimuth angles for longitude and latitude, respectively. $|j, m\rangle$ are the eigenvectors that satisfy the equations $\hat{J}^2 |j, m\rangle = j(j+1)\hbar^2 |j, m\rangle$ and $\hat{J}_z |j, m\rangle = m\hbar |j, m\rangle$ ($\hbar=1$ in numerical calculations). The quantum state can be represented by the Husimi function or the Wigner distribution. The CSS can be prepared by applying $\pi/2$ pulses to a BEC with N atoms in the internal ground state [12–14]. In the CSS, $\langle \hat{J}_x \rangle = N/2$ and $\langle \hat{J}_y \rangle = \langle \hat{J}_z \rangle = 0$. Such a pulse is equivalent to the effect of a beam splitter in an interferometer.

Commencing with a CSS aligned along the x -axis and characterized by isotropic fluctuation in its spin components, \hat{J}_z^2 shears the coherent state to a squeezed one with the reduced variance of \hat{J}_z , culminating in the generation of a spin-squeezed state. Such states exceed the constraints delineated by the standard quantum limit, allowing for enhanced measurement sensitivity in metrology along the squeezed direction [7]. The squeezed direction would be fixed on \hat{J}_z under the action of $\Omega(t)\hat{J}_x$ determined by the RL agent as mentioned above.

B. Prepare spin-squeezed states by machine-designed pulses

Usually, it is hard to avoid decoherence in a quantum system due to its interaction with the environment. The effect of such decoherence should be taken into account in the control scheme. We consider two kinds of decoherence channels: superradiant damping and dephasing. Such decoherence channels lead to the loss of quantum resources. The time evolution of the collective spin system is described by the Lindblad master equation as

$$\dot{\rho} = -i[\hat{H}, \rho] + \gamma(n_{th} + 1)\mathcal{L}_{\hat{J}_-}\rho + \gamma n_{th}\mathcal{L}_{\hat{J}_+}\rho + \gamma_z\mathcal{L}_{\hat{J}_z}\rho, \quad (10)$$

where $\mathcal{L}_{\hat{X}}\rho = 2\hat{X}^\dagger\rho\hat{X} - \hat{X}\hat{X}^\dagger\rho - \rho\hat{X}\hat{X}^\dagger$. γ is the decay rate, γ_z is the dephasing rate and n_{th} is the average thermal photons. Different from the traditional quantum Lyapunov control strategies which are based on the distance between eigenstates [29], the system would evolve under the domain of this master equation with the application of the control field $\Omega(t)$ designed using RL in the Hamiltonian (3).

In this work, the RL agent selects those actions contingent upon the observations, thereby orchestrating a sequence of actions aimed at maximizing cumulative rewards and minimizing penalties. During the training, the observation (calculated based on the quantum state) is fed to the neural network, while output neurons provide the probability of choosing which action at each iterative training step. A reward is dispensed subsequently to each step to evaluate the decision-making policy. After one epoch, the collective spin system is re-initialized to the coherent state and the next epoch starts to train the agent continuously based on the trained neural network. The state evolves deterministically according to the master equation (10). The pulse strengths and application time in the episode represent the policy π^* .

There are means to improve the performance of an RL agent. The replay mechanism stores the learned history in training, and enhances the learning efficiency and stability. Besides, we employ Huber loss in the RL agent [52] since it is robust when the error becomes too large due to the linear function used. For a batch of N samples, the Huber loss is defined as: $L = \{l_1, \dots, l_N\}^T$, where

$$l_n = \begin{cases} \frac{1}{2}e^2 & \text{if } |e| \leq \Delta, \\ \delta(|e| - 0.5 * \Delta) & \text{if } |e| > \Delta, \end{cases} \quad (11)$$

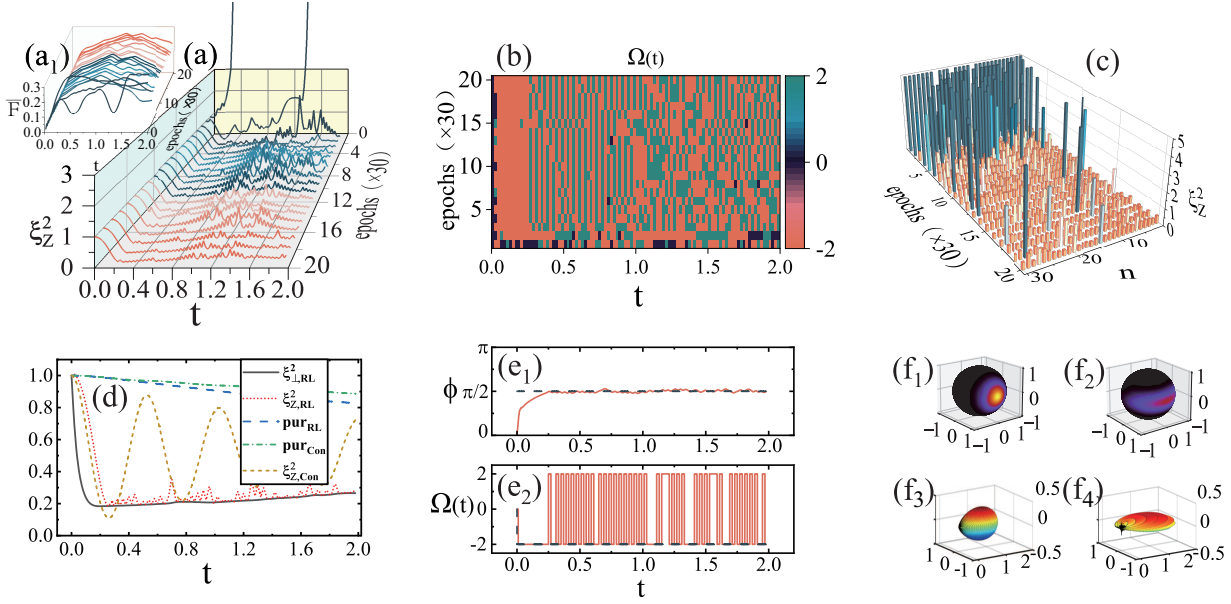


Figure 2. (a) Evolution of the spin squeezing parameter (6) versus training epochs while 100 segments of actions are evenly taken across each evolution time interval $[0, 2]$. Every 30 training epochs are shown within 600 consecutive training rounds. The subfigure in (a₁) shows the evolution of the corresponding averaged QFI defined as $\bar{F} = [F(\rho, \hat{J}_x) + F(\rho, \hat{J}_y) + F(\rho, \hat{J}_z)] / (3N^2)$. (b) Top view of the 3-action ($\Omega(t) = 2, 0, -2$) square control pulse corresponding to the spin squeezing curves in (a). (c) 30 samples (differentiated by n) of the squeezing parameter at $t = 2$ of those in (a). As shown in Fig. (a), there are control sequences causing ξ_Z^2 to diverge at the beginning. However, such control sequences are invalid. Therefore, we express instances where $\xi_Z^2 > 5$ uniformly as 5 to facilitate the visualization of the results in (c). (d) The squeezing parameters versus time for the constant coherent control ($\Omega(t) = -2$) and the RL-designed control, with the corresponding degree of mixing indicated by $\text{Tr}[\rho^2(t)]$. The subscript RL means $\Omega(t)$ obtained by reinforcement learning, Con means $\Omega(t) = -2$. (e₁) evolution of the angle φ in Eq. (5). (e₂) The control fields $\Omega(t)$ designed by the RL agent corresponding to (d) and the constant control field $\Omega(t) = -2$. (f₁) and (f₂) are the Husimi representation of the initial CSS and the spin squeezed state at $t = 2$. (f₃) and (f₄) are the polar plots of the Wigner functions for the states. We use $N = 2J = 20$ hereafter. The decaying parameters are $\gamma = \gamma_z = 0.001\kappa$.

Here, e represents the error term, for instance, the difference between the predicted and actual Q values, $Q(s, a) - Q^*(s, a)$, and Δ is a hyperparameter. It makes the training more stable and provides a balance between Mean Squared Error (underestimates large errors) and Mean Absolute Error (overestimates small errors). It also helps in reducing the exploding gradients problem in training deep neural networks and can potentially lead to faster convergence compared to the other loss functions [52].

The neural network parameters are updated by the descent method called AdamW [53]. The key difference between Adam and AdamW lies in their approach to weight decay which helps prevent over-fitting by adding a penalty term to the loss function. Huber loss and AdamW can be replaced by other loss functions and Optimization algorithms [16, 17].

As a result of this training, the weights of the neural network are adjusted, i.e., the agent learns to determine a sequence of actions based on the states of the system to obtain a larger reward. Randomness provides the probability for the RL agent to find the best sequence of actions.

It is imperative to clarify that the strategy is a closed-loop simulation, but an open-loop application scheme. Once the control sequence of actions, such as $\Omega_x(t)$ delineated in Eq.(3), is obtained by simulation, the identical control field is implemented in an open-loop control process to circumvent quantum collapse attributable to the observation on the system.

VI. CONTROL RESULTS

A. The results of the control method

As depicted in Fig. 2, the time interval $[0, 2]$ is partitioned into a variable number of segments, and the control square pulse is applied at the boundaries between the adjacent time segments and sustained until reaching the subsequent boundary. The RL agent designs the application of the pulses. Each round of the training consists of 600 epochs. Every 30 epochs of the evolution for the squeezing parameter are illustrated in Fig. 2 (a). It can be seen that, at the early stages of the training, the agent does not provide an effective control strategy,

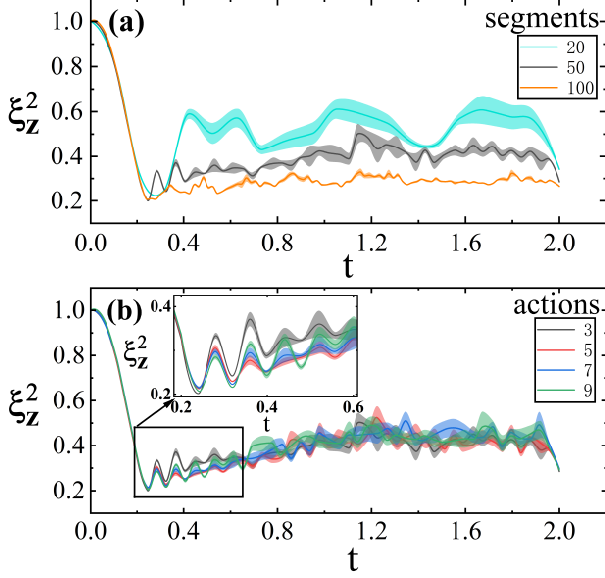


Figure 3. (a) Mean evolution of 30 samples of the spin squeezing parameter ξ_Z^2 . The shaded regions indicate the standard errors of the fits for the different frequencies of applying the control pulses. Control time interval $[0, 2]$ is evenly divided into the number of segments at which the square pulse sequence with amplitude 2 ($\Omega(t) = 2, 0, -2$) is applied. We should confirm that each of the 30 samples is the one with the smallest ξ_Z^2 among the 600 epochs as in Fig. 2. It is reasonable since in practical scenarios, one should choose the best control sequence in experiments. This results in the contraction of the fluctuation error values at time $t = 2$. (b) Evolution of the spin squeezing parameter for different numbers of control actions when the number of segments is 40: $\{\Omega(t)\} = \{(2, 0, -2) | \text{actions} = 3\}$, $\{(2, 1, 0, -1, -2) | \text{actions} = 5\}$, $\{(2, 1.34, 0.66, 0, -0.66, -1.34, -2) | \text{actions} = 7\}$, $\{(2, 1.5, 1, 0.5, 0, -0.5, -1, -1.5, -2) | \text{actions} = 9\}$. The other parameters are the same as those in Fig. 2 (a).

resulting in the divergence of ξ_Z^2 . However, as the training proceeds, the RL agent can find numerous sequences of square pulses inducing a reduction of the squeezing parameter. Meanwhile, the inset Fig. 2 (a_1) delineates the evolution of the corresponding averaged QFI. As the training progresses, \bar{F} tends to attain a high value and descend gradually. This descent corresponds to the increase of ξ_Z^2 resulting from the decoherence. Fig. 2 (b) depicts the corresponding square wave control pulses from the top view. To show the efficacy of the control strategy from another view, Fig. 2 (c) reveals that, upon incrementing the training epochs, there is a discernible decrease in the squeezing parameter at $t = 2$ from the statistical view. These results corroborate the efficacy of the control pulses designed by the RL agent in optimizing the control performance. Fig. 2 (d) presents the evolution of the spin squeezing parameter obtained by using RL-designed $\Omega(t)$: $\xi_{Z,RL}^2$, constant control field $\Omega(t) = -2$: $\xi_{Z,Con}^2$, and the optimized $\xi_{\perp,RL}^2$, with the minimal value

at the final control time $t = 2$ among the 600 epochs. The comparison clearly demonstrates a significantly enhanced performance of the RL-based control approach as opposed to the constant control scenario under the same parameter settings. We employ the trace of the square of the system state $\rho(t)$: $\text{Tr}[\rho^2(t)]$ to describe the degree of mixing for a quantum state. It can be seen that the degree of mixing of the state under the RL control tends to be more deeply compared to $\Omega(t) = -2$. The optimal squeezing angle $\varphi \rightarrow \pi/2$, i.e., converges to the z-component, which can be seen in Fig. 2 (e_1). The linear term $\Omega_x(t)\hat{J}_x$ rotates the fluctuation and \hat{J}_z^2 twist the fluctuation. The combination of these two terms leads to long-lasting spin-squeezed states. The square wave control sequence corresponding to the RL control result in Fig. 2 (d) is depicted in Fig. 2 (e_2). Furthermore, Fig. 2 (f_1) – (f_4) utilize the Husimi function and the Wigner function to visualize the initial coherent spin state and final spin-squeezed state at the time $t = 2$. Nonclassical states are characterized by the twisted distribution in Husimi function [1, 8] and the asymmetry in the polar plot of Wigner function [54, 55]. This provides insight into the evolution of the quantum state under control. To show the squeezing process more vividly, a movie of the squeezing process is shown by Husimi function in [56].

We conjecture that the application frequency of the pulses impacts the outcomes of the control. To investigate the evolution of the squeezing parameter versus different application frequencies, we split the temporal interval $[0, 2]$ into different numbers of segments, the more segments, the more frequently applying the pulses. It can be seen in Fig. 3(a), with increasing the segments, the squeezing parameter is depressed more stationary and lower. Even more, with increasing of the control pulses, the variance of the squeezing parameter is also depressed more obviously. Straightforwardly, there is a contradiction between the control performance and operation difficulty. One may conjecture the number of control actions also influences the control performance. However, as shown in Fig. 3(b), there is no obvious advantage for more control actions with the same maximum control amplitude in this control.

It is natural to ask about the applicability of the proposed scheme to collective spin models with different total spin numbers ($N = 2J$). To address this concern, Fig. 4 (a) illustrates the control result for the collective spin systems with different N s. The result reveals that the squeezing parameter reaches lower values for larger N with the same other parameters. This observation suggests that an enlarged ensemble of spins benefits enhancing the precision of quantum metrology. Furthermore, an examination of the subgraph discloses a convergence towards parallelism among the trajectories corresponding to different N s, indicating an emergence of scaling behavior. In the system under consideration, energy dissipation concurrent with decoherence interplays with the applied coherent pulses which impedes the quantum system decay to the ground state. Consequently, the plateau

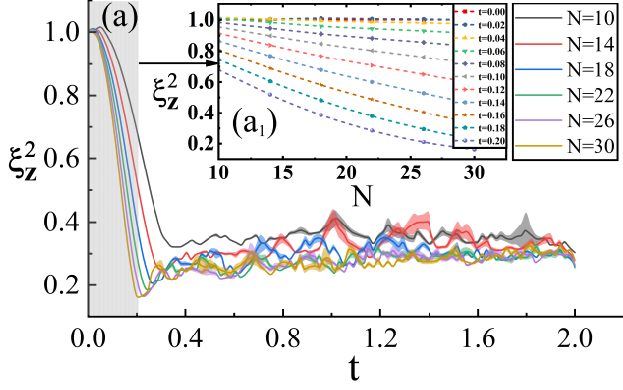


Figure 4. Average evolutions for 30 samples of the spin squeezing parameter ξ_Z^2 with error zones for different sizes of the collective spin system $N = 2J$ under 3-action ($\Omega(t) = 2, 0, -2$) control. The samples are picked in the same manner as those shown in Fig. 3 (a). The subgraph shows the squeezing parameter in the scaled time interval $t = [0, 0.2]$, picked from the shaded area on the left in the graph, for the collective spin system of different sizes. The same color is shared with the same N . The other parameters are same to those in Fig. 2 (a).

in the squeezing parameter can be attributed to the dynamic equilibrium between these two conflicting factors.

In the previous results, the environmental temperature was assumed to be zero. To investigate the robustness of the proposed control scheme, it is necessary to check the influence of temperature on the control result. Since the temperature is positively correlated with the average number of thermal excitations in the reservoir, denoted by n_{th} , it reflects the strength of the decoherence. Fig. 5 illustrates that an incremental rise of the thermal excitation impairs the efficacy of the control strategy from the view of spin squeezing and the control variance.

B. The comparison with current protocols

In the two-component weakly interacting Bose-Einstein condensate [12], the minimum value for the squeezing parameter $\xi^2 = N(\Delta\hat{J}_{\vec{n}_1})^2/(\langle\hat{J}_{\vec{n}_2}\rangle^2 + \langle\hat{J}_{\vec{n}_3}\rangle^2)$ approaches $\frac{1}{2}(3/N)^{2/3}$ at an optimized direction. In the work [57], a BEC of thousands ^{87}Rb atoms can be described by the one-axis twisting Hamiltonian $\hat{H} = E_C/2\hat{J}_z^2 - 2E_J/N\hat{J}_x$, where the Josephson energy E_J characterizes the tunneling between the two condensates, and the charging energy E_C describes the repulsive interaction inside BEC. The squeezing parameter $\xi_N^2 = \xi_R^2 \cos \varphi^2 = \Delta\hat{J}_z^2/\Delta\hat{J}_{z,\text{ref}}^2$ is used to describe squeezing, where φ is the phase difference of the two modes. The concurrent presence of number squeezing and high phase coherence enabled the spin squeezing parameter $\xi_R^2 = -3.8\text{dB}$ for the two main well pairs of a six-well lattice (approximately 2,200 atoms), and

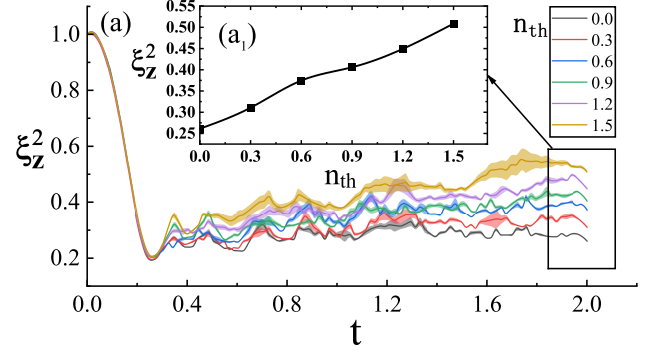


Figure 5. The average evolutions of 30 squeezing parameters with error zones for different thermal excitations in the reservoir with $n_{th} = \frac{1}{\exp(\hbar\omega/k_B T) - 1}$: the average number of photons for a mode with frequency ω in the reservoir. The samples are picked in the same manner as those shown in Fig. 3 (a). The subgraph shows the squeezing parameter versus average thermal excitation at the scaled time $t = 2$. The other parameters are the same as those in Fig. 2 (a).

$\xi_R^2 = -2.3\text{dB}$ for the double-well configuration (approximately 1,600 atoms). In a similar BEC of ^{87}Rb (total number 2,300) nonlinear Ramsey interferometer experiments [13], the minimal number squeezing factor $\xi_N^2 = 4(\Delta\hat{J}_z)^2/N = -8.2_{-1.2}^{+0.8}\text{dB}$ after taking the technical noise due to coupling-pulse imperfections and magnetic field fluctuations into account. In another work [14], spin squeezing was generated in an atom chip by controlling the elastic collision interactions, resulting to $\xi_R^2 = -2.5_{0.6}^{-0.6}\text{dB}$ for 1250 ± 45 atoms.

Theoretically, a scheme using repeated Rabi pulses transforming one-axis-twisting model to two-axis-twisting type with the Hamiltonian $\hat{H}(t) = \chi\hat{J}_z^2 + \Omega(t)\hat{J}_y$, and the squeezing parameter $\xi^2 = 2(\Delta\hat{J}_{min})^2/J = 4(\Delta\hat{J}_{min})^2/N$ can approach the Heisenberg limited $1/N$ [58]. In another protocol using the chopped random basis technique [59], the squeezing parameter $\xi^2 = N(\Delta\hat{J}_x)^2/|\langle\hat{J}_z\rangle|^2 \sim 2.1/N^{0.94}$ with a time-random-fluctuation Hamiltonian. In a four-step strategy including constant-value and time-varying controls to prepare spin squeezing for an ensemble of the two-level systems coupled to a single-mode bosonic field, when $N = 2J = 8$, the squeezing parameter $\xi^2 = 2(\Delta\hat{J}_{min})^2/J$ can approach -8dB [21]. In these proposals, the optimized spin squeezing occurs at certain time and phase angles.

According to our results in Fig. 3, Fig. 4, and Fig. 5, the squeezing parameter $\xi_Z^2 = N\Delta\hat{J}_z^2/|\langle\hat{J}_z\rangle|^2$ can be stabilized in the range of -5dB to -7dB for a long time. Compared with the current works, the advantage of our scheme lies in its ability to provide spin-squeezed states along \hat{J}_z over a longer time window without the need to extract squeezed states at a specific squeezing time. Moreover, we have considered quantum mechanical dissipation, making our theoretical research closer to actual experimental scenarios.

VII. DISCUSSIONS

A. Experimental feasibility

As mentioned above, atomic BEC are promising platforms for implementing the control protocol. In the current experiments, the condensate ensemble can be effectively modeled as the collective pseudo-spin model described by (3) [13, 14, 60]. In these experiments, hyperfine states of the condensed atoms play the role of the spin-up and spin-down states. The nonlinear term \hat{J}_z^2 is contingent upon the normalized density overlap of the two BEC components and can be modulated via Feshbach resonance. The Rabi frequency $\Omega(t)$ is essential in our proposal, and can be realized by a $\pi/2$ microwave pulse coupling the near-resonant two-photon hyperfine states of a ^{87}Rb BEC trapped in optical lattice [13, 14]. The Rabi frequency can be turned rapidly between 0 and $2\pi \times 600\text{Hz}$, enabling swift state manipulation [13, 14]. Our protocol requires no additional modifications to existing experimental setups, except for a timing sequence of the Rabi pulses. Therefore, we anticipate that our protocol can be implemented with current experimental techniques.

B. Application to continuous variable systems

Continuous variable systems, characterized by their extensive degrees of freedom, typically present greater challenges in terms of control. Nonetheless, it has been demonstrated that Deep DRL can effectively address continuous-space control challenges even in the presence of measurement back-action noise [61]. Continuous position measurement on the particle leads to state reduction and can be stabilized employing measurement-based feedback control [62]. For DRL, the continuous position measurement acts as the input of the neural network. To design the control field, the differential equation of the expectations would be used, instead of the quantum density matrix directly. Although the controlled system and quantities may be continuous, the control field can be pulsed.

C. Application to other quantum system

The operations are acting on all particles identically in the interferometer. In the large N (the number of particles) limit, the collective spin model can also be mapped to the bosonic model by the Holstein-Primakoff transformation: $\hat{J}_z = N/2 - \hat{c}^\dagger \hat{c} \simeq N/2$ and $\hat{J}_+ = (N - \hat{c}^\dagger \hat{c})^{1/2} \hat{c} \simeq \sqrt{N} \hat{c}$, where \hat{c} (\hat{c}^\dagger) is a bosonic annihilation (creation) operator [63]. This mapping hints that we can apply

the control proposal to such quantum systems to pursue quantum resources.

D. Replaceability of the reinforcement learning module

DQN is employed as an implementation of the control scheme, actually the RL agent can be replaced by other modules possessing similar learning functions. Several candidates capable of substituting the RL agent have been identified and evaluated. For example, the State-Action-Reward-State-Action algorithm [35], Deep Deterministic Policy Gradient [36], Asynchronous Advantage Actor-Critic [37], Dueling Network [38] and so on.

Reinforcement learning provides a tool to optimize the dynamics of a quantum system. The optimal criterion varies for different control targets. The principle of using this scheme is that the controlled systems evolve under certain mapping rules (differential equations). And the optimal module just finds the road to the optimal goal more efficiently. After all, the machine-learning agents learn the patterns or mappings based on the statistical distributions.

VIII. CONCLUSION

In conclusion, we have proposed a reinforcement-learning-based control strategy to generate non-classical collective spin states in an open environment. The machine learning agent can design a suite of control sequences to prepare spin-squeezed states accompanied by entanglement. We find larger frequency of applying the pulses enhances the performance of the control strategy. However, more choices of actions do not contribute obviously to the control outcomes. The scalability of this framework is demonstrated, facilitating its applicability to larger systems. Notably, thermal excitations progressively undermine the control performance. The control proposal can be realized within current experiments of atomic Bose-Einstein condensates. The extensions of the control paradigm to continuous control problems and other quantum systems are discussed. The versatility of this scheme is underlined by the potential of substituting the reinforcement learning agent with other optimization modules.

IX. ACKNOWLEDGEMENTS

X. L. Zhao thanks discussions with Li Jiachun and Hou Shaocheng, Natural Science Foundation of Shandong Province, China, No.ZR2020QA078, No.ZR2023MD064, and National Natural Science Foundation of China, No.12005110, No.12074206.

[1] J. Ma, X. G. Wang, C. P. Sun, and F. Nori, *Physics Reports* **509**, 89 (2011).

[2] L. Pezzè, A. Smerzi, M. K. Oberthaler, R. Schmied, and P. Treutlein, *Rev. Mod. Phys.* **90**, 035005 (2018).

- [3] D. J. Wineland, J. J. Bollinger, W. M. Itano, F. L. Moore, and D. J. Heinzen, *Phys. Rev. A* **46**, R6797 (1992).
- [4] D. J. Wineland, J. J. Bollinger, W. M. Itano, and D. J. Heinzen, *Phys. Rev. A* **50**, 67 (1994).
- [5] R. J. Sewell, M. Koschorreck, M. Napolitano, B. Dubost, N. Behbood, and M. W. Mitchell, *Phys. Rev. Lett.* **109**, 253605 (2012).
- [6] A. D. Ludlow, M. M. Boyd, J. Ye, E. Peik, and P. O. Schmidt, *Rev. Mod. Phys.* **87**, 637 (2015).
- [7] L. Pezzé, and Augusto Smerzi, *Phys. Rev. Lett.* **102**, 100401 (2009).
- [8] M. Kitagawa and M. Ueda, *Phys. Rev. A* **47**, 5138 (1993).
- [9] A. Kuzmich, N. P. Bigelow, and L. Mandel, *Europhys. Lett.* **42**, 481 (1998).
- [10] C. K. Law, H. T. Ng, and P. T. Leung, *Phys. Rev. A* **63**, 055601 (2001).
- [11] L. M. Duan, A. Sørensen, J. I. Cirac, and P. Zoller, *Phys. Rev. Lett.* **85**, 3991 (2000).
- [12] A. Sørensen, L. M. Duan, J. L. Cirac, and P. Zoller, *Nature* **409**, 63 (2001).
- [13] C. Gross, T. Zibold, E. Nicklas, J. Estève, and M. K. Oberthaler, *Nature* **464**, 1165(2010).
- [14] M. F. Riedel, P. Böhi, Y. Li, T. W. Hänsch, A. Sinatra, and P. Treutlein, *Nature* **464**, 1170(2010).
- [15] J. Biamonte, P. Wittek, N. Pancotti, P. Rebentrost, N. Wiebe, and S. Lloyd, *Nature* **549**, 195 (2017).
- [16] K. P. Murphy, *Machine Learning: A Probabilistic Perspective*, MIT Press (2012).
- [17] R. S. Sutton and A. G. Barto, *Reinforcement learning: An introduction*, MIT Press (2018).
- [18] T. Fösel, P. Tighineanu, T. Weiss, and F. Marquardt, *Phys. Rev. X* **8**, 031084 (2018).
- [19] V. Dunjko, and H. J. Briegel, *Reports on Progress in Physics* **81**, 074001 (2018).
- [20] S. Yu, F. Albarrán-Arriagada, J. C. Retamal, Y. T. Wang, W. Liu, Z.J. Ke, Y. Meng, Z. P. Li, J. S. Tang, E. Solano, L. Lamata, C.F. Li, and G.C. Guo, *Adv. Quantum Technol* **2**, 1800074 (2019).
- [21] Q. S. Tan, M. Zhang, Y. Chen, J. Q. Liao, and J. Liu, *Phys. Rev. A* **103**, 032601 (2021).
- [22] F. Albarrán-Arriagada, J. C. Retamal, E. Solano, and L. Lamata, *Phys. Rev. A* **98**, 042315 (2018).
- [23] L. Viola and S. Lloyd *Phys. Rev. A* **58**, 2733 (1998).
- [24] S. C. Hou, M. A. Khan, X. X. Yi, Daoyi Dong, and Ian R. Petersen, *Phys. Rev. A* **86**, 022321 (2012).
- [25] S. Grivopoulos, and B. Bamieh, In *Proceedings of the 42nd IEEE conference on decision and control* **1**, 434 (2003).
- [26] M. Mirrahimi, P. Rouchon, and G. Turinici, *Automatica* **41**, 1987 (2005).
- [27] R. V. Handel, J. K. Stockton, and H. Mabuchi, *IEEE Trans. Automat. Control* **50**, 768 (2005).
- [28] X. X. Yi, S. L. Wu, C. F. Wu, X. L. Feng, and C. H. Oh, *J. Phys. B: At. Mol. Opt. Phys.* **44**, 195503 (2011).
- [29] X. L. Zhao, Y. L. Ma, H. Y. Ma, T. H. Qiu, and X. X. Yi, *Physics Letters A* **425**, 127874 (2022).
- [30] V. Mnih, K. Kavukcuoglu, D. Silver, A. A. Rusu, J. Veness, M. G. Bellemare, A. Graves, M. Riedmiller, A. K. Fidjeland, G. Ostrovski, S. Petersen, C. Beattie, A. Sadik, I. Antonoglou, H. King, D. Kumaran, D. Wierstra, S. Legg, and D. Hassabis, *Nature* **518**, 529 (2015).
- [31] R. Bellman, *Proc. Natl. Acad. Sci.* **38**, 716 (1952).
- [32] Y. LeCun, Y. Bengio, and G. Hinton, *Nature* **521**, 436 (2015).
- [33] I. Goodfellow, Y. Bengio, and A. Courville, *Deep learning*, MIT Press(2016).
- [34] M. Hessel, J. Modayil, H. v. Hasselt, T. Schaul, G. Ostrovski, W. Dabney, D. Horgan, B. Piot, M. Azar, and D. Silver, In *Proceedings of the 30nd AAAI Conference on Artificial Intelligence* **32**, 1 (2018); arXiv:1710.02298.
- [35] G. A. Rummery, and M. Niranjan, <https://api.semanticscholar.org/CorpusID:59872172> (1994).
- [36] D. Silver, G. Lever, N. Heess, T. Degris, D. Wierstra, and M. Riedmiller, *Proceedings of the 31st International Conference on Machine Learning*, PMLR **32**, 387(2014).
- [37] V. Mnih, A. P. Badia, M. Mirza, A. Graves, T. P. Lillicrap, T. Harley, D. Silver, and K. Kavukcuoglu, arXiv:1602.01783(2016).
- [38] Z. Wang, T. Schaul, M. Hessel, H. v. Hasselt, M. Lanctot, and N. d. Freitas, *Proceedings of The 33rd International Conference on Machine Learning*, PMLR **48**, 1995 (2016).
- [39] F. T. Arecchi, E. Courtens, R. Gilmore, and H. Thomas, *Phys. Rev. A* **6**, 2211 (1972).
- [40] L. G. Biedenharn, and J. C. Louck, *Angular Momentum in Quantum Physics Theory and Application*, (Addison-Wesley, Reading, MA, 1981).
- [41] L. Song, X. Wang, D. Yan, Z. Zong, *J. Phys. B: At. Mol. Opt. Phys.* **39** 559(2006).
- [42] A. S. Sørensen, and K. Mølmer, *Phys. Rev. Lett.* **86**, 4431 (2001).
- [43] G. Tóth, *Phys. Rev. A* **85**, 022322 (2012).
- [44] C. W. Helstrom, *J. Stat. Phys.* **1**, 231(1969).
- [45] H. Strobel, W. Muessel, D. Linnemann, T. Zibold, D. B. Hume, L. Pezzé, A. Smerzi, and M. K. Oberthaler, *Science* **345**, 424 (2014).
- [46] C. W. Helstrom, *Phys. Lett. A* **25**, 101 (1967).
- [47] S. L. Braunstein and C. M. Caves, *Phys. Rev. Lett.* **72**, 3439 (1994).
- [48] Y. M. Zhang, X. W. Li, W. Yang, and G. R. Jin, *Phys. Rev. A* **88**, 043832 (2013).
- [49] J. Liu, X. X. Jing, and X. G. Wang *Sci. Rep.* **5**, 8565 (2015).
- [50] P. Hyllus, W. Laskowski, R. Krischek, C. Schwemmer, W. Wieczorek, H. Weinfurter, L. Pezzé, and A. Smerzi, *Phys. Rev. A* **85**, 022321 (2012).
- [51] M. Zhang, H. M. Yu, H. D. Yuan, X. G. Wang, R. D. Dobrzański, and J. Liu, *Phys. Rev. Research* **4**, 043057 (2022).
- [52] P. J. Huber, *Annals of Mathematical Statistics* **35**, 73(1964).
- [53] I. Loshchilov and F. Hutter, <https://arxiv.org/abs/1711.05101>.
- [54] M. G. Benedict, and A. Czirják, *Phys. Rev. A* **60**, 4034 (1999).
- [55] T. Tilma, M. J. Everitt, J. H. Samson, W. J. Munro, and K. Nemoto, *Phys. Rev. Lett.* **117**, 180401(2016).
- [56] A movie shows the squeezing process by Husimi function.
- [57] J. Estève, C. Gross, A. Weller, S. Giovanazzi, and M. K. Oberthaler, *Nature* **455**, 1216 (2008).
- [58] Y. C. Liu, Z. F. Xu, G. R. Jin, and L. You, *Phys. Rev. Lett.* **107**, 013601 (2011).
- [59] T. Pichler, T. Caneva, S. Montangero, M. D. Lukin, and T. Calarco, *Physical Review A* **93**, 013851 (2016).
- [60] G. R. Jin and S. W. Kim, *Phys. Rev. Lett.* **99**, 170405 (2007).

- [61] Z. T. Wang, Y. Ashida, and M. Ueda, Phys. Rev. Lett. **125**, 100401 (2020).
- [62] L. Disi, Phys. Lett. A **129**, 419 (1988).
- [63] T. Holstein and H. Primakoff, Phys. Rev. **58**, 1098 (1940).